Boundaries for Efficient Use of Electron Vortex Beams to Measure Magnetic Properties

Ján Rusz[1,2,*] and Somnath Bhowmick[1,3]

[1]Department of Physics and Astronomy, Uppsala University, Post Office Box 516, 75120 Uppsala, Sweden
[2]Institute of Physics, Czech Academy of Sciences, Na Slovance 2, 182 21 Prague, Czech Republic
[3]Department of Materials Science and Engineering, Indian Institute of Technology, Kanpur 208016, India

(Received 16 June 2013; published 6 September 2013)

Development of experimental techniques for characterization of magnetic properties at high spatial resolution is essential for progress in miniaturization of magnetic devices, for example, in data storage media. Inelastic scattering of electron vortex beams (EVBs) was recently reported to contain atom-specific magnetic information. We develop a theoretical description of inelastic scattering of EVBs on crystals and perform simulations for EVBs of different diameters. We show that use of an EVB wider than an interatomic distance does not provide any advantage over an ordinary convergent beam without angular momentum. On the other hand, in the atomic-resolution limit, electron energy loss spectra measured by EVBs are strongly sensitive to the spin and orbital magnetic moments of studied matter, when channeling through or very close to the atomic columns. Our results demonstrate the boundaries for efficient use of EVBs in measurement of magnetic properties.

DOI: 10.1103/PhysRevLett.111.105504 PACS numbers: 61.05.J−, 41.20.Jb, 41.85.−p, 42.50.Tx

For several decades, data storage technologies have been in tireless evolution to keep up with the processing of ever-increasing amounts of data. The technology behind data storage relies to a large fraction on the magnetic properties of materials. Reducing the dimensions of magnetic bits to the nanometer scale naturally requires characterization techniques that provide the means to measure magnetic properties at desired spatial resolution. This resolution is slowly getting out of reach for x-ray-based techniques, such as x-ray magnetic circular dichroism. In 2006, an analogous technique, but performed with transmission electron microscope, was discovered [1]—the electron magnetic circular dichroism (EMCD). EMCD relates spin and orbital magnetic moments to a difference of electron energy loss spectra measured at specific crystal orientations. As an electron-microscopy-based technique, it brought a promise of element-sensitive magnetic characterization at atomic resolution. Since then, EMCD went through a rapid development with significant improvements both in spatial resolution and signal-to-noise ratio [2–5]. Early adopters have successfully used it in their applications [6–12]. Yet, EMCD has not reached a stage of a wide spread as a routine characterization technique. The major obstacle is a low signal-to-noise ratio, which is due to the fact that EMCD needs to be measured on crystals at scattering directions between the transmitted beam and Bragg spots.

In an attempt to overcome these difficulties, Verbeeck *et al.* [13] have used electron vortex beams (EVBs [14,15]) to measure an EMCD signal. This experiment suggests that EMCD can be measured at a transmitted beam, if the beam would carry an angular momentum. Provided we could obtain EVBs with an intensity comparable to an "ordinary" convergent electron beam [16], this would lead to EMCD spectra with a substantially enhanced signal-to-noise ratio. The recipe is simple: one should measure an electron energy loss spectrum with an EVB with angular momentum $\langle \hat{L}_z \rangle = +\hbar$ and another one with an EVB with $\langle \hat{L}_z \rangle = -\hbar$, and their difference should provide an EMCD spectrum.

Theoretical developments have followed [17–24] and provided understanding of formation of EVBs, their elastic scattering on crystals, and inelastic scattering on individual atoms. A common feature of these works is a focus on EMCD at an atomic resolution, which naturally demands atomic-size vortex beams. A question of using EVBs for magnetic characterization at the mesoscopic scale (about 1 nm and beyond, in the present context) has not been studied, despite its great potential for applications. What is also missing is an understanding of an inelastic interaction of EVBs with matter—an assembly of atoms—a key question for applying EVBs for EMCD measurements. From the experimental point of view, quite surprisingly, further works utilizing EVBs for measurement of EMCD have not appeared in literature so far. A lack of follow-up experiments and an incomplete theoretical understanding motivated us to explore theoretically and computationally the inelastic scattering of EVBs on magnetic materials.

In this Letter, we develop a theory of inelastic scattering of EVBs on matter. Using the body-centered cubic crystal of iron as a benchmark structure, we show that sensitivity of the EVBs to magnetic moments crucially depends on its diameter. We demonstrate that the EVB is efficient for detection of EMCD only in the atomic-resolution limit, where it provides a higher signal-to-noise ratio than the *intrinsic* EMCD method [1] relying on dynamical diffraction.

The initial EVB wave function was generated in reciprocal space by $\phi(q,\varphi) = e^{im\varphi}\Theta(q_{\max} - q)$, where $q = \sqrt{k_x^2 + k_y^2}$, φ is the azimuthal angle, orbital angular momentum $\langle \hat{L}_z \rangle = \hbar m$, Θ is the Heaviside function, and $q_{\max}$ determines the radius of the disk in the reciprocal space [20]. We adopted two values of $q_{\max}$, namely, 0.1 a.u.$^{-1}$, representing a beam much wider than one unit cell (referred to as the wide beam) and $q_{\max} = 0.5$ a.u.$^{-1}$, representing a beam substantially narrower than the distance between the adjacent atomic columns in bcc iron (the narrow beam). It has been demonstrated that such atom-sized EVBs are within reach [21,25]. The initial wave function was propagated through a bcc-iron crystal along the (001) direction up to a thickness of 40 nm using a multislice method [26], assuming an acceleration voltage of 200 keV. For both beam diameters, we have considered three values of angular momentum of the beam $\langle \hat{L}_z \rangle = -\hbar$, 0, $\hbar$ and scanned the whole area of the unit cell by varying the lateral position of the beam center.

Development of the EVB angular momentum as a function of illumination spot and sample thickness was already studied in Ref. [20]. We extend these results by considering two different beam diameters and showing the range of angular momenta that EVBs can reach at a particular sample thickness; see Fig. 1. We find a dramatically different behavior of wide vs narrow beams—forecasting our main result concerning the inelastic electron scattering further below.

The angular momentum of a wide beam is practically independent of the illumination spot [see the minimum-maximum intervals in Fig. 1(a)]. This can be qualitatively predicted, knowing that the diameter of the beam covers several unit cells. In contrast, for a narrow beam, the exchange of angular momentum between the beam and lattice is very sensitive to the illumination spot, as indicated by a large spread of values in Fig. 1(b).

In addition, we note that a beam with nonzero angular momentum can be obtained by propagating a narrow beam with $\langle \hat{L}_z \rangle = 0$ through a crystal of suitable thickness, provided one can pass a narrow probe through an appropriate lateral position within the unit cell. Beyond 10 nm, at certain illumination spots, it acquires a non-negligible angular momentum, reaching a peak of value $\sim 0.5\hbar$ at a thickness of 20 nm. However, an averaged value over the whole unit cell remains zero at all thicknesses [Fig. 1(b)]. For a beam with orbital angular momentum $\langle \hat{L}_z \rangle = \hbar$, the average over the unit cell does not vanish within the thickness range considered in our simulations. As in the case of a beam with $m = 0$, it is possible to manipulate the probe's angular momentum by illuminating an appropriate spot in the unit cell and passing the beam through a sample of suitable thickness. Note that the range of accessible values is substantially enhanced compared to a probe with zero initial $\langle \hat{L}_z \rangle$.

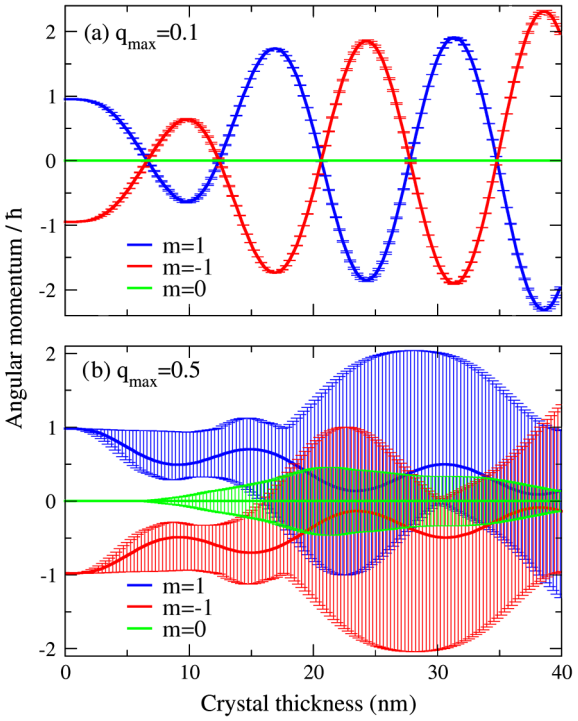

FIG. 1 (color online). Evolution of $\langle \hat{L}_z \rangle$ of the vortex beam as a function of sample thickness, averaged over different locations of the vortex core within a unit cell. "Error bars" indicate the spread of the angular momenta (minimum and maximum) at a given thickness. The top panel shows that a wide beam with $q_{\max} = 0.1$ has a negligible spread and thus virtually no dependence of angular momentum on the position of the vortex core. For a narrow vortex beam (bottom panel, $q_{\max} = 0.5$), there is a large spread of the angular momenta.

The probe wave functions calculated by the multislice method serve as an input for the inelastic electron scattering calculations [27]. We have employed the *operator maps* technique [28] for evaluation of the inelastic scattering matrix elements of the L_3 edge of bcc iron (energy loss 708 eV). This method allows us to split the L_3-edge integrated inelastic scattering cross section into a contribution due to holes in the $3d$ shell (referred to as the nonmagnetic signal) and a contribution due to spin and orbital magnetic moments (i.e., EMCD integrated over the L_3 edge, or the magnetic signal). Technical details of the computational method will be reported elsewhere [29].

A striking result is obtained for the wide vortex beam $q_{\max} = 0.1$. Like in the case of exchange of angular momentum with lattice, the simulations show that the energy-filtered diffraction (EFDIF) patterns are independent of the position of the vortex center within the unit cell. Moreover, and this constitutes one of the main results of this Letter, these EFDIF patterns are independent of the angular momentum of EVBs. In other words, for a wide vortex beam, there is no influence of the beam vorticity on the observed diffraction patterns, which rules

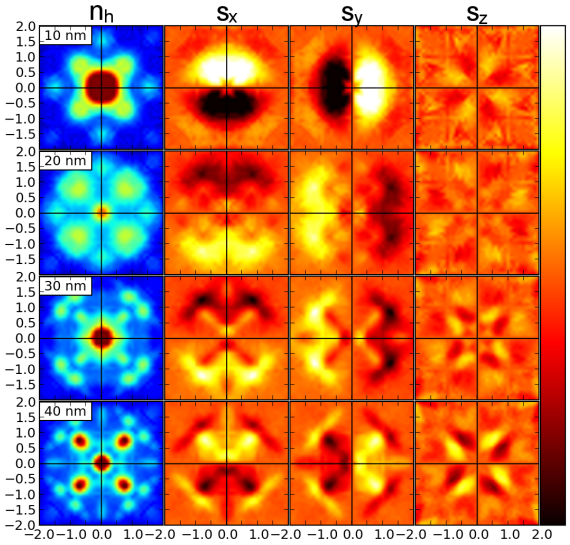

FIG. 2 (color online). Inelastic scattering of a wide vortex beam. The grid of EFDIF patterns shows intensity per hole in a $3d$ shell and per Bohr magneton of spin magnetization in the x, y, and z directions (columns from left to right) for four different thicknesses, 10, 20, 30, and 40 nm (rows from top to bottom). Range of plots is from $-2G$ to $2G$, where $\mathbf{G} = (100)$. The color ranges are from 0 to 3.0 (blue to red) for the first column and -0.0625 to 0.0625 (black to yellow) for the second to fourth columns, respectively.

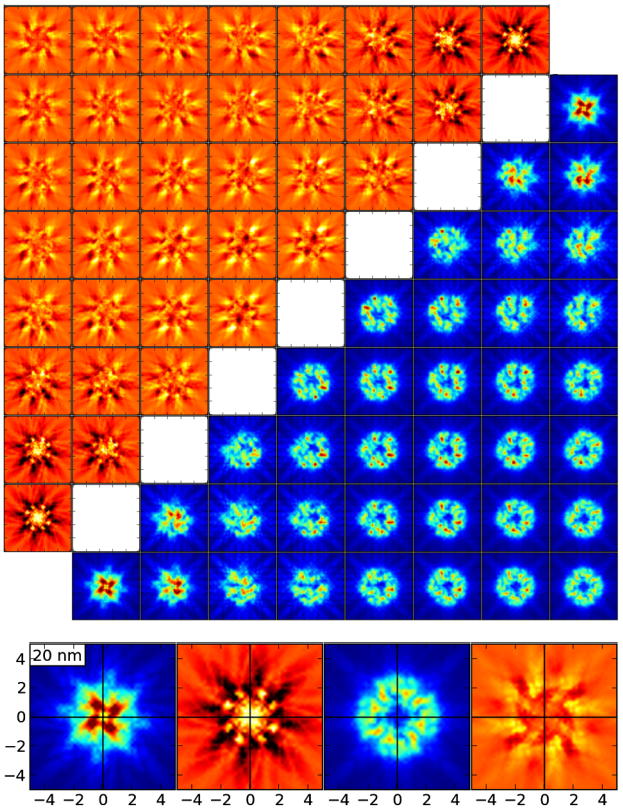

FIG. 3 (color online). Inelastic scattering of a narrow vortex beam with angular momentum $\langle \hat{L}_z \rangle = +\hbar$, calculated for a sample thickness of 20 nm. Figure displays a grid of calculated EFDIF patterns normalized per hole in a $3d$ shell (right-bottom triangle) and per Bohr magneton of magnetization in the z direction (left-top triangle), representing the nonmagnetic and magnetic signals, respectively. The color ranges are from 0 to 1.2 (dark blue to red) and -0.025 to 0.025 (black to yellow), respectively. The range of plots is from $-5G$ to $5G$ in both the x and y directions, where $\mathbf{G} = (100)$. The maps in the lower-left corner correspond to a vortex core passing through an atom at the origin of the unit cell, while the maps in the right-top corner describe a vortex passing through a column of atoms in the centers of the body-centered cubic unit cells. The bottom panel shows the diffraction patterns (nonmagnetic and magnetic parts) for a vortex passing through an atomic column (left) and in between columns (right).

out the utility of EVBs for measuring magnetic signal beyond atomic resolution. Representative EFDIF patterns are shown in Fig. 2. Note that there is a non-negligible magnetic signal present in the diffraction plane for all three directions of magnetization. However, this signal originates solely from dynamical diffraction effects; i.e., it is an *intrinsic* EMCD appearing due to the crystal itself acting as a beam splitter [1]. In the light of these findings, we suggest that the EMCD signal observed by Verbeeck *et al.* [13] was of intrinsic origin.

For the narrow beam, we observe rich and featureful dynamical diffraction effects. Inelastic scattering sensitively depends on the position of the vortex center within the unit cell, as is demonstrated in Fig. 3, showing EFDIF patterns for 36 positions of the EVB core from a triangular wedge mapping $1/8$ of the area of the crystal unit cell. The development of the shape of the diffraction pattern is rather nontrivial, both for the nonmagnetic and magnetic contributions. Magnetic signal is particularly strong when the EVB passes close to the atom columns (bottom-left and top-right corners of Fig. 3).

The EFDIF patterns as a function of an illumination spot allow us to evaluate high-resolution energy-filtered images [30] (HR-EFI) which conveniently summarize the second main result of this Letter. We have simulated the detector aperture by a circle of radius $0.6G$ and $3.2G$ [$\mathbf{G} = (100)$] for the wide and narrow beams, respectively. These values are approximately equal to the $q_{\max}$ used to generate initial wave functions.

Calculations for the wide beam did not produce any contrast within the unit cell, as mentioned above. The nonmagnetic signal is independent of a position of the EVB core, and the magnetic signal vanishes after integration over an aperture—regardless of the angular momentum of the beam and magnetization directions.

For the narrow beam, we have plotted the HR-EFI in Fig. 4. Results for the beam with zero angular momentum show well-resolved positions of atomic columns. A nonzero magnetic signal can be detected; however, it is of very low relative magnitude below 0.3%. In the case of a vortex

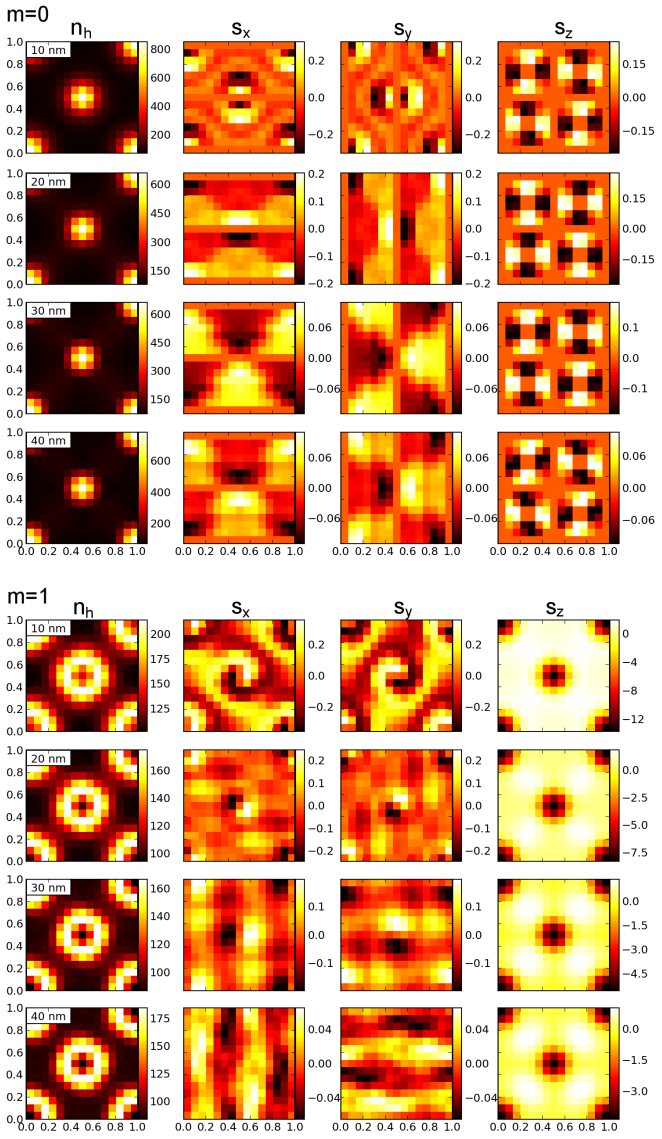

FIG. 4 (color online). High-resolution energy-filtered images for a beam of zero angular momentum (top panel) and $\langle \hat{L}_z \rangle = \hbar$ (bottom panel). Individual rows correspond to thicknesses of 10, 20, 30, and 40 nm, respectively, and columns refer to signal contributions normalized per hole or per $1\mu_B$ of spin magnetization along the x, y, and z directions, respectively. Each pattern covers one unit cell.

beam with $\langle \hat{L}_z \rangle = \hbar$, the maximum strength of the nonmagnetic signal is reduced. It can be explained by a more spread beam of doughnut shape, which also leads to a lower spatial resolution—note the wider atomic columns in the nonmagnetic component of HR-EFI for a vortex beam, compared to a beam with zero angular momentum (left columns of the upper and lower panels of Fig. 4). On the other hand, the magnetic signal originating from the magnetic moment along the z direction is much more localized and significantly stronger than for a beam with $\langle \hat{L}_z \rangle = 0$.

This shows that for a sufficiently narrow EVB channeling through an atomic column (in our case, within 0.6 Å from the atomic column), the intensity of inelastically scattered EVBs in the forward direction is substantially influenced by magnetic moments within the atomic column. At certain probe positions, at 10 nm, the magnetic signal reaches 10% of the maximum nonmagnetic signal. In comparison to the intrinsic EMCD, where the net EMCD signal in the case of bcc Fe does not exceed 0.5% of the transmitted beam intensity [31], this is a significantly stronger signal and remains stronger within the studied range of thicknesses up to 40 nm.

Importantly, an integral of HR-EFI over the area of the whole unit cell provides very weak magnetic signals of the order of less than 0.05% of the nonmagnetic signal. Therefore, our calculations demonstrate that in order to utilize EVBs for measurement of EMCD, one has to scan the crystal at an atomic resolution. Only in this case, there is a theoretical possibility to measure an enhanced magnetic signal with an EVB, but this is yet to be demonstrated experimentally.

In conclusion, we have demonstrated the range of applicability of EVBs for measuring magnetic properties of matter. Our results should stimulate further development of EVB experiments at an atomic resolution, which could become the method of choice for element-specific magnetic characterization of thin crystalline layers.

J. R. acknowledges the Swedish Research Council, Göran Gustafsson's Foundation, the Swedish National Infrastructure for Computing (NSC Center), and computer cluster DORJE at the Czech Academy of Sciences.

*jan.rusz@physics.uu.se

[1] P. Schattschneider, S. Rubino, C. Hébert, J. Rusz, J. Kuneš, P. Novák, E. Carlino, M. Fabrizioli, G. Panaccione, and G. Rossi, Nature (London) **441**, 486 (2006).

[2] P. Schattschneider, C. Hébert, S. Rubino, M. Stöger-Pollach, J. Rusz, and P. Novák, Ultramicroscopy **108**, 433 (2008).

[3] B. Warot-Fonrose, F. Houdellier, M.J. Hÿtch, L. Calmels, V. Serin, and E. Snoeck, Ultramicroscopy **108**, 393 (2008).

[4] P. Schattschneider, M. Stöger-Pollach, S. Rubino, M. Sperl, C. Hurm, J. Zweck, and J. Rusz, Phys. Rev. B **78**, 104413 (2008).

[5] H. Lidbaum, J. Rusz, S. Rubino, A. Liebig, B. Hjörvarsson, P. M. Oppeneer, O. Eriksson, and K. Leifer, Ultramicroscopy **110**, 1380 (2010).

[6] Z. H. Zhang, X. Wang, J. B. Xu, S. Muller, C. Ronning, and Q. Li, Nat. Nanotechnol. **4**, 523 (2009).

[7] R. F. Klie, T. Yuan, M. Tanase, G. Yang, and Q. Ramasse, Appl. Phys. Lett. **96**, 082510 (2010).

[8] M. Stöger-Pollach, C. D. Treiber, G. P. Resch, D. A. Keays, and I. Ennen, Micron **42**, 456 (2011).

[9] Z. H. Zhang, H. L. Tao, M. He, and Q. Li, Scr. Mater. **65**, 367 (2011).

[10] J. Salafranca, J. Gazquez, N. Pérez, A. Labarta, S. T. Pantelides, S. J. Pennycook, X. Batlle, and M. Varela, Nano Lett. **12**, 2499 (2012).
[11] B. Loukya, X. Zhang, A. Gupta, and R. Datta, J. Magn. Magn. Mater. **324**, 3754 (2012).
[12] Z. Q. Wang, X. Y. Zhong, R. Yu, Z. Y. Cheng, and J. Zhu, Nat. Commun. **4**, 1395 (2013).
[13] J. Verbeeck, H. Tian, and P. Schattschneider, Nature (London) **467**, 301 (2010).
[14] M. Uchida and A. Tonomura, Nature (London) **464**, 737 (2010).
[15] B. J. McMorran, A. Agrawal, I. M. Anderson, A. A. Herzing, H. J. Lezec, J. J. McClelland, and J. Unguris, Science **331**, 192 (2011).
[16] P. Schattschneider, M. Stöger-Pollach, and J. Verbeeck, Phys. Rev. Lett. **109**, 084801 (2012).
[17] J. C. Idrobo and S. J. Pennycook, J. Electron Microsc. **60**, 295 (2011).
[18] S. M. Lloyd, M. Babiker, and J. Yuan, Phys. Rev. A **86**, 023816 (2012).
[19] S. M. Lloyd, M. Babiker, and J. Yuan, Phys. Rev. Lett. **108**, 074802 (2012).
[20] S. Löffler and P. Schattschneider, Acta Crystallogr., Sect. A: Found. Crystallogr. **68**, 443 (2012).
[21] P. Schattschneider, B. Schaffer, I. Ennen, and J. Verbeeck, Phys. Rev. B **85**, 134422 (2012).
[22] H. L. Xin and H. Zheng, Microsc. Microanal. **18**, 711 (2012).
[23] A. Lubk, L. Clark, G. Guzzinati, and J. Verbeeck, Phys. Rev. A **87**, 033834 (2013).
[24] J. Yuan, S. M. Lloyd, and M. Babiker, arXiv:1303.5322.
[25] J. Verbeeck, P. Schattschneider, S. Lazar, M. Stoger-Pollach, S. Loffler, A. Steiger-Thirsfeld, and G. Van Tendeloo, Appl. Phys. Lett. **99**, 203109 (2011).
[26] E. J. Kirkland, *Advanced Computing in Electron Microscopy* (Springer, New York, 2010), 2nd ed..
[27] J. Rusz, S. Muto, and K. Tatsumi, Ultramicroscopy **125**, 81 (2013).
[28] J. Rusz, S. Rubino, O. Eriksson, P. M. Oppeneer, and K. Leifer, Phys. Rev. B **84**, 064444 (2011).
[29] J. Rusz and S. Bhowmick (to be published).
[30] M. P. Prange, M. P. Oxley, M. Varela, S. J. Pennycook, and S. T. Pantelides, Phys. Rev. Lett. **109**, 246101 (2012).
[31] S. Muto, K. Tatsumi, and J. Rusz, Ultramicroscopy **125**, 89 (2013).